

# X-ray Survey Results on Active Galaxy Physics and Evolution

W.N. Brandt,<sup>1</sup> D.M. Alexander,<sup>2</sup> F.E. Bauer,<sup>2</sup> and C. Vignali<sup>3</sup>

<sup>1</sup> Department of Astronomy & Astrophysics, The Pennsylvania State University, 525 Davey Lab, University Park, PA 16802, USA ([niel@astro.psu.edu](mailto:niel@astro.psu.edu))

<sup>2</sup> Institute of Astronomy, Madingley Road, Cambridge CB3 0HA, UK ([dma@ast.cam.ac.uk](mailto:dma@ast.cam.ac.uk), [feb@ast.cam.ac.uk](mailto:feb@ast.cam.ac.uk))

<sup>3</sup> INAF—Osservatorio Astronomico di Bologna, Via Ranzani 1, 40127 Bologna, Italy ([cristian@anastasia.bo.astro.it](mailto:cristian@anastasia.bo.astro.it))

## 1 Introduction

The cosmic X-ray background (XRB) is largely due to accretion onto supermassive black holes integrated over cosmic time. Thus, extragalactic X-ray surveys offer the potential to contribute substantially to our understanding of the physics of Active Galactic Nuclei (AGN) as well as the evolution of the AGN population. Such surveys have dramatically advanced over the past four years, largely due to the flood of data from the *Chandra X-ray Observatory* (hereafter *Chandra*) and the *X-ray Multi-Mirror Mission-Newton* (hereafter *XMM-Newton*). The superb X-ray mirrors and charge-coupled device (CCD) detectors on these observatories provide

- Sensitive imaging spectroscopy in the  $\approx 0.5$ –10 keV band, with up to 50–250 times (depending upon the energy band considered) the sensitivity of previous X-ray missions. X-ray surveys have finally reached the depths needed to complement the most sensitive surveys in the radio, submillimeter, infrared, and optical bands.
- X-ray source positions with accuracies of  $\approx 0.3$ –3". These high-quality positions are essential for matching to (often faint) multiwavelength counterparts.
- Large source samples allowing reliable statistical inferences to be drawn about the overall extragalactic X-ray source population. In a fairly deep *Chandra* or *XMM-Newton* observation,  $\gtrsim 100$ –200 sources can be detected.

The extragalactic survey capabilities of *Chandra* and *XMM-Newton* are complementary in several important respects. The sub-arcsecond imaging of *Chandra* provides the best possible source positions, and with long exposures *Chandra* can achieve the highest possible sensitivity at energies of  $\approx 0.5$ –6 keV; unlike the case for *XMM-Newton*, even the deepest *Chandra* observations performed to date do not suffer from significant source confusion. *XMM-Newton*, in comparison, has a substantially larger photon collecting area than *Chandra*, allowing efficient X-ray spectroscopy. In addition,

**Table 1.** Some Deep X-ray Surveys with *Chandra* and *XMM-Newton*

Survey Name	Exposure	Representative Reference or Note
<i>Chandra</i>		
<i>Chandra</i> Deep Field-North	1950 ks	D.M. Alexander et al., 2003, AJ, 126, 539
<i>Chandra</i> Deep Field-South	940 ks	R. Giacconi et al., 2002, ApJS, 139, 369
HRC Lockman Hole	300 ks	PI: Murray
Extended CDF-S	250 ks	PI: Brandt
Groth-Westphal	200 ks	PI: Nandra
Lynx	185 ks	D. Stern et al., 2002, AJ, 123, 2223
LALA Cetus	177 ks	PI: Malhotra
LALA Boötes	172 ks	J.X. Wang et al., 2004, AJ, 127, 213
SSA13	101 ks	A.J. Barger et al., 2001, AJ, 121, 662
3C295	100 ks	V. D’Elia et al., 2004, astro-ph/0403401
Abell 370	94 ks	A.J. Barger et al., 2001, AJ, 122, 2177
SSA22 “protocluster”	78 ks	L.L. Cowie et al., 2002, ApJ, 566, L5
ELAIS	75 ks	J.C. Manners et al., 2003, MNRAS, 343, 293
WHDF	75 ks	PI: Shanks
<i>XMM-Newton</i>		
Lockman Hole	766 ks	G. Hasinger et al., 2001, A&A, 365, L45
<i>Chandra</i> Deep Field-South	317 ks	A. Streblyanska et al., 2004, astro-ph/0309089
13 hr Field	200 ks	M.J. Page et al., 2003, AN, 324, 101
<i>Chandra</i> Deep Field-North	180 ks	T. Miyaji et al., 2003, AN, 324, 24
Subaru Deep	100 ks	PI: Watson
ELAIS S1	100 ks	PI: Fiore
Groth-Westphal	80 ks	T. Miyaji et al., 2004, astro-ph/0402617

The Extended *Chandra* Deep Field-South is comprised of four fields (each 250 ks), the *XMM-Newton* ELAIS S1 survey is comprised of four fields (each 100 ks), and the *Chandra* ELAIS survey is comprised of two fields (each 75 ks). The *XMM-Newton* Subaru Deep survey also has seven flanking fields (each  $\approx 50$  ks). Only the first  $\approx 100$  ks of the *XMM-Newton* Lockman Hole data have been published at present.

*XMM-Newton* has better high-energy response than *Chandra* and can carry out the deepest possible surveys from  $\approx 7$ –10 keV. Even *XMM-Newton*, however, does not cover the peak of the X-ray background at 20–40 keV. Finally, the field of view for *XMM-Newton* is  $\sim 2.5$  times that of *Chandra*.

*Chandra* and *XMM-Newton* have resolved  $\gtrsim 80$ –90% of the 0.5–10 keV XRB into discrete sources, extending earlier heroic efforts with missions including *ROSAT*, *ASCA*, and *BeppoSAX*. The main uncertainties in the precise resolved fraction are due to field-to-field cosmic variance (which leads to spatial variation in the XRB flux density) and instrumental cross-calibration limitations. With the recent advances, attention is now focused on (1) understanding the nature of the X-ray sources in detail and their implications for AGN physics, and (2) understanding the cosmological evolution of the

Due to astro-ph file size limitations,  
 this figure is only available from  
<http://www.astro.psu.edu/users/niel/papers/papers.html>

**Fig. 1.** Adaptively smoothed image of the 2 Ms CDF-N, constructed from data in the 0.5–2 keV (red), 2–4 keV (green), and 4–8 keV (blue) bands. Nearly 600 sources are detected in the  $\approx 448$  arcmin<sup>2</sup> field. The regions covered by the HDF-N and GOODS-N surveys are denoted. Adapted from D.M. Alexander, F.E. Bauer, W.N. Brandt, et al., 2003, AJ, 126, 539.

sources and their role in galaxy evolution. In this review, we briefly describe the key *Chandra* and *XMM-Newton* extragalactic surveys to date (§2) and detail some of their implications for AGN physics and evolution (§3). In §3 we highlight two topics of current widespread interest: (1) X-ray constraints on the AGN content of luminous submillimeter galaxies, and (2) the demography and physics of high-redshift ( $z > 4$ ) AGN as revealed by X-ray observations. We also discuss prospects for future X-ray surveys with *Chandra*, *XMM-Newton*, and upcoming missions (§4).

Throughout this paper, we adopt  $H_0 = 70$  km s<sup>-1</sup> Mpc<sup>-1</sup>,  $\Omega_M = 0.3$ , and  $\Omega_\Lambda = 0.7$  (flat cosmology).

## 2 Chandra and XMM-Newton Extragalactic Surveys

To learn about AGN physics and evolution in a complete manner, both “deep” and “wider” X-ray surveys are required; the trade-off between the two, of course, is between sensitivity and solid-angle coverage on the sky. None of the *Chandra* and *XMM-Newton* surveys discussed in this paper is truly wide-field, in that the widest still only cover  $\lesssim 1\%$  of the sky.<sup>4</sup> Both deep and wider X-ray surveys are reviewed briefly below.

### 2.1 Deep X-ray Surveys

Table 1 makes it clear that deep *Chandra* and *XMM-Newton* surveys are a major “industry.” The 21 surveys listed there have a total exposure exceeding 70 days, and  $\gtrsim 50$  scientists have invested substantial effort on the analysis and interpretation of these data. Comparable effort has also been expended on multiwavelength follow-up studies of these surveys; due to the small solid angles under investigation, superb multiwavelength coverage can be obtained relatively economically.

The two most sensitive surveys in Table 1, by a significant factor, are the 2 Ms *Chandra* Deep Field-North (CDF-N; see Figure 1) and 1 Ms *Chandra* Deep Field-South (CDF-S). Both are situated in intensively studied regions of sky with little Galactic foreground X-ray absorption. They reach 0.5–2 keV fluxes of  $\approx (2.5\text{--}5)\times 10^{-17}$  erg cm<sup>-2</sup> s<sup>-1</sup>, corresponding to count rates of  $\lesssim 1$  count every 2–4 days. At these flux levels, even moderate-luminosity AGN (similar to Seyfert galaxies in the local universe) can be detected to  $z \gtrsim 10$ . The CDF-N and CDF-S are clearly “pencil-beam” surveys, each covering  $\approx 400$  arcmin<sup>2</sup>; for reference, this is  $\sim 1/2$  the solid angle of the full Moon and  $\sim 75$  times the solid angle of the original Hubble Deep Field-North (HDF-N; see Figure 1). Public X-ray source catalogs are available for both the CDF-N and CDF-S (see the references in Table 1); these contain  $\approx 580$  and  $\approx 370$  sources, respectively.

The other deep X-ray surveys in Table 1 have generally been performed in regions of sky where (1) extensive coverage already exists at one-to-several wavelengths, and/or (2) some interesting astronomical object is present (e.g., 3C295, Abell 370, or the SSA22 “protocluster”). They are all sensitive enough to detect moderate-luminosity AGN to  $z \sim 3\text{--}5$ , and in total the surveys in Table 1 cover a solid angle of  $\sim 3.5$  deg<sup>2</sup> ( $\sim 16$  Moons).

### 2.2 Wider X-ray Surveys

Wider *Chandra* and *XMM-Newton* surveys (see Table 2) are a comparably large and important “industry” to the deep surveys. These typically involve

<sup>4</sup> For this reason, we denote these surveys as “wider” (relative to the deep *Chandra* and *XMM-Newton* surveys) rather than “wide-field.”

**Table 2.** Some Wider X-ray Surveys with *Chandra* and *XMM-Newton*

Survey Name	$\Omega$ (deg <sup>2</sup> )	Representative Reference or Note
<i>Chandra</i>		
ChaMP	14	D.W. Kim et al., 2004, ApJS, 150, 19
Clusters Serendipitous	1.1	P. Gandhi et al., 2004, MNRAS, 348, 529
CYDER	...	F.J. Castander et al., 2003, AN, 324, 40
Lockman Hole NW	0.4	A.T. Steffen et al., 2003, ApJ, 596, L23
MUSYC	1	PI: van Dokkum
NOAO DWFS	9.3	PI: Jones
SEXSI	2.2	F.A. Harrison et al., 2003, ApJ, 596, 944
SWIRE Lockman	0.6	PI: Wilkes
1 hr Field	0.2	PI: McHardy
13 hr Field	0.2	I.M. McHardy et al., 2003, MNRAS, 342, 802
<i>XMM-Newton</i>		
AXIS	...	X. Barcons et al., 2002, A&A, 382, 522
CFRS	0.6	T.J. Waskett et al., 2003, MNRAS, 341, 1217
HELLAS2XMM	2.9	A. Baldi et al., 2002, ApJ, 564, 190
LSS	64	M. Pierre et al., 2004, astro-ph/0305191
Survey Science Center	...	M.G. Watson et al., 2001, A&A, 365, L51
VIMOS	2.3	PI: Hasinger
2dF	1.5	A. Georgakakis et al., 2003, MNRAS, 344, 161

The second column above lists estimated survey solid angles; survey sensitivities are not uniform but rather vary significantly across these solid angles. In some cases, survey solid angles are not well defined and thus are not listed. In these cases, the reader should consult the listed reference or note for further details.

investigation of X-ray sources in  $\sim 4$ –150 X-ray observations of moderate exposure (usually 20–60 ks, but sometimes as short as  $\approx 5$  ks); the observations are sometimes obtained from the public data archives. The wider surveys serve to bridge the observational “gap” between the deepest *Chandra* observations and the deepest observations made by previous X-ray missions (e.g., *ROSAT*; see Figure 2), and they effectively target the intermediate 0.5–8 keV flux levels ( $10^{-15}$ – $10^{-13}$  erg cm<sup>-2</sup> s<sup>-1</sup>) which contribute most significantly to the XRB.

The wider X-ray surveys provide a broad census of the X-ray source population, often generating enormous numbers of sources (1000–6000 or more; e.g., see Figure 2). They thereby allow discovery of both intrinsically rare source types as well as low-redshift examples of sources found in the deep X-ray surveys. However, complete multiwavelength follow-up often must be compromised for reasons of observational economy; thus many of the wider surveys target specific source types of interest. Often targeted are sources with unusually hard X-ray spectra, sources with unusually large X-ray-to-optical flux ratios, or sources that appear likely to be at high redshift based upon optical imaging data.

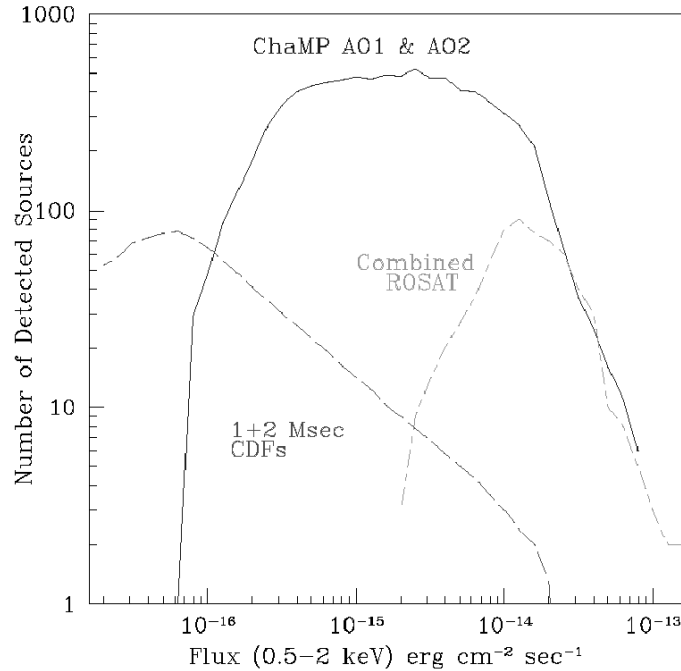


**Fig. 2.** Number of sources predicted from the ChaMP survey (for 137 ChaMP fields from *Chandra* Cycle 1 and Cycle 2) compared to numbers of sources from the *Chandra* Deep Fields and the *ROSAT* surveys analyzed by T. Miyaji, G. Hasinger, & M. Schmidt, 2000, *A&A*, 353, 25. An impressive  $\approx 6000$  ChaMP sources are expected in total, and these largely lie at intermediate 0.5–2 keV flux levels of  $(4\text{--}60)\times 10^{-16}$  erg cm $^{-2}$  s $^{-1}$ . From D.W. Kim, R.A. Cameron, J.J. Drake, et al., 2004, *ApJS*, 150, 19.

### 3 Some Implications for AGN Physics and Evolution

#### 3.1 Properties of the X-ray Sources

##### Basic Nature

A broad diversity of X-ray sources is found in the recent *Chandra* and *XMM-Newton* surveys. This is apparent in even basic flux-flux plots such as that shown in Figure 3; at the faintest X-ray flux levels in the CDF-N, the extragalactic sources range in optical flux by a factor of  $\gtrsim 10,000$ .

Classification of the X-ray sources is challenging for several reasons. First of all, many of the sources are simply too faint for efficient optical spectroscopic identification with 8–10 m class telescopes (note the small dots in Figure 3). Intensive optical identification programs on the deepest *Chandra* and *XMM-Newton* fields typically have  $\approx 50\text{--}70\%$  completeness at best.

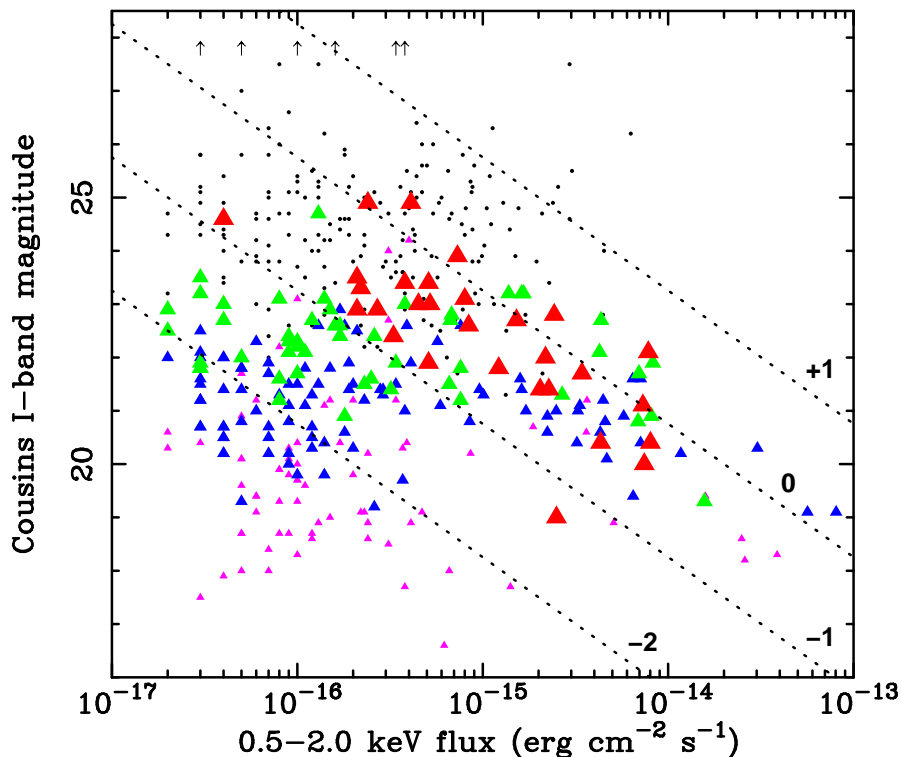


**Fig. 3.** *I*-band magnitude versus 0.5–2 keV flux for extragalactic X-ray sources in the CDF-N. Sources with redshifts of 0–0.5, 0.5–1, 1–2, and 2–6 are shown as violet, blue, green, and red filled triangles, respectively (symbol sizes also increase with redshift). Small black dots indicate sources without measured redshifts. The slanted, dotted lines indicate constant values of  $\log(f_X/f_I)$ ; the respective  $\log(f_X/f_I)$  values are labeled. Adapted from D.M. Alexander, F.E. Bauer, W.N. Brandt, et al., 2003, *AJ*, 126, 539 and A.J. Barger, L.L. Cowie, P. Capak, et al., 2003, *AJ*, 126, 632.

Furthermore, many of the X-ray sources have modest apparent optical luminosities, and thus their host galaxies make substantial diluting contributions to the flux measured in a spectroscopic aperture. Finally, another challenge is an apparent “schism” between optical (type 1 vs. type 2) and X-ray (unobscured vs. obscured) schemes of classification; not all X-ray obscured AGN have type 2 optical spectra, and not all AGN with type 1 optical spectra are unobscured.

Considering X-ray, optical, and multiwavelength information, the primary extragalactic source types are found to be the following:

- *Unobscured AGN.* Blue, broad-line AGN are found that do not show signs of obscuration at either X-ray or optical/UV wavelengths. They are found over a broad range of redshift ( $z \approx 0$ –5), and they comprise a significant

Due to astro-ph file size limitations,  
 this figure is only available from  
<http://www.astro.psu.edu/users/niel/papers/papers.html>

**Fig. 4.** *Chandra* and *HST* images of the HDF-N. The 22 *Chandra* sources are circled on the *HST* image; the circles are much larger than the *Chandra* source positional errors. The numbers are source redshifts; redshifts followed by a “p” are photometric. Basic source type information for many of the sources is also given.

fraction of the brightest X-ray sources. At  $z \gtrsim 1.5$  they also comprise a substantial fraction of all X-ray sources with spectroscopic identifications (certainly in part because these objects are the most straightforward to identify spectroscopically).

- *Obscured AGN with clear optical/UV AGN signatures.* Some objects showing X-ray evidence for obscuration have clear AGN signatures in their rest-frame optical/UV spectra. Notably, such AGN can have both type 1 and type 2 optical/UV classifications. Most of these objects have  $z \lesssim 1.5$ .
- *Optically faint X-ray sources.* These sources have  $I \gtrsim 24$  and thus usually cannot be identified spectroscopically. Many, however, appear to be luminous, obscured AGN at  $z \approx 1-3$  when their X-ray properties, optical photometric properties (including photometric redshifts), and multiwavelength properties are considered. Thus, these objects largely represent an extension of the previous class to higher redshifts and fainter optical magnitudes.



- *X-ray bright, optically normal galaxies (XBONGs)*. XBONGs have X-ray luminosities ( $\approx 10^{41}$ – $10^{43}$  erg s $^{-1}$ ) and X-ray-to-optical flux ratios suggesting some type of moderate-strength AGN activity. Some also have hard X-ray spectral shapes suggesting the presence of X-ray obscuration. Optical spectra give redshifts of  $z \approx 0.05$ – $1$ , but AGN emission lines and non-stellar continua are not apparent. The nature of XBONGs remains somewhat mysterious. Some may just be Seyfert 2s where dilution by host-galaxy light hinders optical detection of the AGN, but others have high-quality follow up and appear to be truly remarkable objects. These “true” XBONGs may be (1) AGN with inner radiatively inefficient accretion flows, or (2) AGN that suffer from heavy obscuration covering a large solid angle ( $\approx 4\pi$  sr), so that optical emission-line and ionizing photons cannot escape the nuclear region.
- *Starburst galaxies*. At the faintest X-ray flux levels in the deepest *Chandra* surveys, a significant fraction of the detected sources appear to be  $z \approx 0$ – $1.3$  dusty starburst galaxies. They are members of the strongly evolving starburst population responsible for creating much of the infrared background. The observed X-ray flux appears to be the integrated emission from many X-ray binaries and supernova remnants.
- *“Normal” galaxies*. Apparently normal galaxies are also detected in the deepest *Chandra* surveys out to  $z \approx 0.2$ . The observed X-ray emission is again probably largely from X-ray binaries and supernova remnants; these objects and the starburst galaxies above are probably not distinct but rather constitute a single population of galaxies with star formation of varying intensity. Low-luminosity AGN are likely present in some cases as well. Some normal galaxies sport luminous X-ray sources clearly offset from their nuclei. At even fainter X-ray flux levels, normal and starburst galaxies should be the dominant class of extragalactic X-ray sources.

Most of the AGN found in X-ray surveys are “radio quiet” in the sense that the ratio ( $R$ ) of their rest-frame 5 GHz and 4400 Å flux densities are  $R < 10$ .

Figure 4 shows some of the source classifications in the HDF-N, which is at the center of the CDF-N (see Figure 1) and thus has the most sensitive X-ray coverage available. Note, for example, that three of the brightest X-ray sources are XBONGs. These were not recognized as AGN prior to the *Chandra* observations, despite the many intensive studies of the HDF-N.

### Luminosity and Redshift Distributions

The combined results from deep and wider X-ray surveys show that the sources comprising most of the XRB have X-ray luminosities comparable to those of local Seyfert galaxies, such as NGC 3783, NGC 4051, and NGC 5548 (e.g., see Figure 5). While a few remarkable obscured quasars have been found, these appear fairly rare and only make a small contribution to the

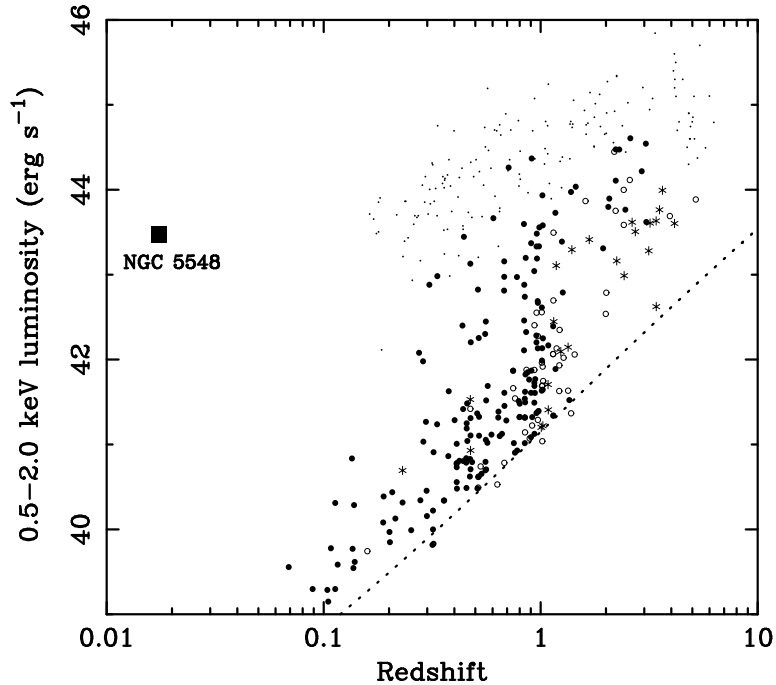


**Fig. 5.** Luminosity in the 0.5–2 keV band (computed from the 0.5–2 keV flux assuming a power-law spectrum with a photon index of  $\Gamma = 2$ ) versus redshift for extragalactic sources in the CDF-N with spectroscopic redshifts. Sources with  $I = 16$ –22,  $I = 22$ –23, and  $I > 23$  are indicated with filled circles, open circles, and stars, respectively. The dotted curve shows the approximate sensitivity limit near the center of the CDF-N. Also shown are the well-studied Seyfert 1 galaxy NGC 5548 (filled square) and Sloan Digital Sky Survey (SDSS) quasars from the SDSS Early Data Release with X-ray coverage in archival *ROSAT* data (small dots; the relevant solid angle covered by pointed *ROSAT* observations is  $\approx 15 \text{ deg}^2$ ). Note that NGC 5548 could have been detected to  $z \sim 10$  in the CDF-N. Note also that the CDF-N and SDSS populations are nearly disjoint, as a consequence of the different solid angle coverages (a factor of  $\sim 120$ ) and depths. Adapted from D.M. Alexander, F.E. Bauer, W.N. Brandt, et al., 2003, *AJ*, 126, 539; A.J. Barger, L.L. Cowie, P. Capak, et al., 2003, *AJ*, 126, 632; and C. Vignali, W.N. Brandt, & D.P. Schneider, 2003, *AJ*, 125, 433.

XRB. Indeed, it appears that the fraction of obscured AGN drops with luminosity from  $\approx 60$ –70% at Seyfert luminosities to  $\approx 30\%$  at quasar luminosities.

Most spectroscopically identified AGN in the deep X-ray surveys have  $z \lesssim 2$ , although a significant minority have  $z \approx 2$ –5. This is partly due to spectroscopic incompleteness bias, as is apparent by comparing the filled circles, open circles, and stars in Figure 5. However, as will be described further

in §3.2, there is a real enhancement of AGN at  $z \lesssim 1$  relative to expectations from pre-*Chandra* AGN-synthesis models of the XRB. An impressive  $\sim 60\%$  of the 2–8 keV XRB arises at  $z < 1$ .

### AGN Sky Density

Most ( $\approx 70\text{--}100\%$ ) of the extragalactic X-ray sources found in both the deep and wider X-ray surveys with *Chandra* and *XMM-Newton* are AGN of some type. Starburst and normal galaxies make increasing fractional contributions at the faintest X-ray flux levels, but even in the CDF-N they represent  $\lesssim 20\text{--}30\%$  of all sources (and create  $\lesssim 5\%$  of the XRB). The observed AGN sky density in the deepest X-ray surveys is  $\approx 6500 \text{ deg}^{-2}$ , about an order of magnitude higher than that found at any other wavelength. This exceptional effectiveness at finding AGN arises because X-ray selection (1) has reduced absorption bias and minimal dilution by host-galaxy starlight, and (2) allows concentration of intensive optical spectroscopic follow-up upon high-probability AGN with faint optical counterparts (i.e., it is possible to probe further down the luminosity function).

### Completeness of X-ray AGN Selection

Are there significant numbers of luminous AGN that are not found even in the deepest X-ray surveys? This could be the case if there is a large population of AGN that are X-ray weak due either to absorption or an intrinsic inability to produce X-rays. This question can be partially addressed by looking for AGN found at other wavelengths that are not detected in X-rays. In the CDF-N, one of the most intensively studied regions of sky at all wavelengths, there are only 1–2 such AGN known. The most conspicuous is 123725.7+621128, a radio-bright ( $\approx 6 \text{ mJy}$  at 1.4 GHz) wide angle tail source that is likely at  $z \approx 1\text{--}2$  (although the redshift of this source remains uncertain). This is one of the brightest radio sources in the CDF-N but has been notoriously difficult to detect in X-rays. Manual analysis of the 2 Ms *Chandra* data at the AGN position indicates a likely, but still not totally secure, detection (at a false-positive probability threshold of  $3 \times 10^{-5}$  using the standard *Chandra* wavelet source detection algorithm). The 0.5–2 keV luminosity is  $\lesssim 5 \times 10^{41} \text{ erg s}^{-1}$ . The only other known AGN in the CDF-N without an X-ray detection is 123720.0+621222, a narrow-line AGN at  $z = 2.45$ ; its 0.5–2 keV luminosity is  $\lesssim 2 \times 10^{42} \text{ erg s}^{-1}$ .

Despite the spectacular success of X-ray surveys at finding AGN, appropriate humility is required when assessing the AGN selection completeness of even the deepest X-ray surveys. This is made clear by consideration of “Compton-thick” AGN, which comprise a sizable fraction ( $\approx 40\%$ ) of AGN in the local universe. Such AGN are absorbed by intrinsic column densities of  $N_{\text{H}} \gg 1.5 \times 10^{24} \text{ cm}^{-2}$ , within which direct line-of-sight X-rays are effectively

destroyed via the combination of Compton scattering and photoelectric absorption. Such AGN are often only visible via weaker, indirect X-rays that are “reflected” by neutral material or “scattered” by ionized material.<sup>5</sup> Many of the local Compton-thick AGN (e.g., NGC 1068, NGC 6240, Mrk 231), if placed at  $z \gtrsim 0.5$ –1.5, would remain undetected in even the deepest *Chandra* surveys. Thus, it appears plausible that  $\approx 40\%$  of AGN at such redshifts may have been missed (the number, of course, could be higher or lower if the fraction of Compton-thick AGN evolves significantly with redshift). Deeper observations with *Chandra* ( $\approx 10$  Ms; see §4.1) may be able to detect the indirect X-rays from any missed Compton-thick AGN, and observations with *Spitzer* may be able to detect “waste heat” from such objects at infrared wavelengths.

Another way to address AGN selection completeness in X-ray surveys is to consider “book-keeping” arguments: can the observed sources explain the observed 20–40 keV XRB intensity, and can all the observed accretion account for the local density of supermassive black holes? The answer is plausibly “yes” in both cases, but with some uncertainty. In the first case, one must make a significant spectral extrapolation from 5–10 keV and worry about mission-to-mission cross-calibration uncertainties. In the second, significant uncertainties remain in bolometric correction factors, accretion efficiencies, and the local density of supermassive black holes. The current book-keeping arguments cannot rule out the possibility that a significant fraction of the AGN population (e.g., Compton-thick AGN) is still missed in X-ray surveys. Indeed, some book-keepers find better agreement with the local black-hole mass function after making a substantial correction for missed accretion in Compton-thick AGN.

### 3.2 Recent X-ray Results on AGN Evolution

Optical studies of AGN evolution have typically focused on luminous quasars. These have been known to evolve strongly with redshift since  $\sim 1968$ , having a comoving space density at  $z \approx 2$  that is  $\gtrsim 100$  times higher than at  $z \approx 0$ . Figure 6a shows optical luminosity functions in 6 redshift “shells” spanning  $z = 0.40$ –2.10 for  $\sim 16,800$  luminous AGN from the 2dF and 6dF surveys. Clear positive evolution with redshift is observed, and pure luminosity evolution (PLE) models provide an acceptable fit to these data. New optical AGN surveys, such as COMBO-17, have recently discovered significant numbers of moderate-luminosity AGN (with  $M_B > -23$ ) at  $z \approx 1$ –4, allowing investigation of their evolution. As for luminous quasars, the AGN found in these

<sup>5</sup> In some “translucent” cases, where the column density is only a few  $\times 10^{24}$   $\text{cm}^{-2}$  (i.e., a few Thomson depths), direct “transmission” X-rays from a Compton-thick AGN may become visible above rest-frame energies of  $\sim 10$  keV. For comparison, the column density through your chest is  $\sim 1 \times 10^{24}$   $\text{cm}^{-2}$ ; if you stood along the line-of-sight to an AGN, you could almost render it Compton thick!

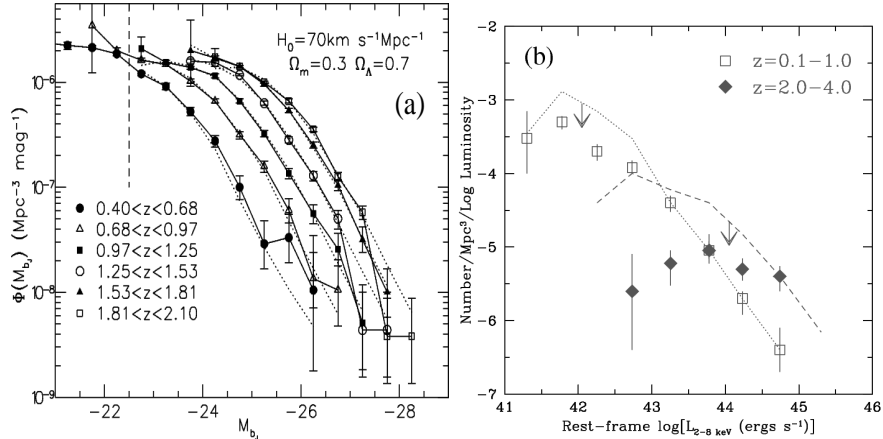


**Fig. 6.** (a) Optical luminosity functions in 6 redshift “shells” spanning  $z = 0.40$ – $2.10$  for  $\sim 16,800$  luminous AGN from the 2dF and 6dF surveys. Note the clear positive evolution with increasing redshift at high luminosity (i.e., the comoving number density of luminous AGN increases with redshift from  $z = 0.40$ – $2.10$ ). From S.M. Croom, R.J. Smith, B.J. Boyle, et al., 2004, MNRAS, in press (astro-ph/0403040). (b) X-ray (2–8 keV) luminosity functions in two redshift “shells” (as labeled) for moderate-to-high luminosity AGN from the CDF-N, Abell 370, SSA13, and SSA22 *Chandra* surveys (see Table 1) as well as several earlier X-ray surveys. The dotted and dashed curves show the maximum possible luminosity functions after allowing for incompleteness of the follow-up spectroscopy. Note the apparent negative evolution with increasing redshift at moderate luminosity. Adapted from L.L. Cowie, G.P. Garmire, M.W. Bautz, et al., 2002, ApJ, 566, L5.

surveys also appear to peak in comoving space density at  $z \approx 2$ . Both PLE and pure density evolution (PDE) models can acceptably fit the COMBO-17 data alone. Although a systematic combination of the COMBO-17 data with a large sample of higher-luminosity AGN has yet to be published, there are hints that the redshift at which the comoving space density peaks is smaller at lower luminosities.

As noted in §3.1, the deepest X-ray surveys efficiently select AGN even fainter than those found by COMBO-17 out to high redshift (e.g., see Figure 5). X-ray AGN samples show a clear dependence of AGN evolution upon luminosity, with strong positive evolution only being seen at high luminosities (see Figure 6b). Lower luminosity AGN appear to be about as common at  $z \approx 0$ – $1$  as they ever were, consistent with trend hinted at by COMBO-17. These results are robust to incompleteness of the spectroscopic follow up, although clearly they are still dependent upon the completeness of AGN X-ray selection (see §3.1). It appears that while the SMBH in rare, luminous AGN could grow efficiently at high redshift, the SMBH in most AGN had to wait longer to grow.

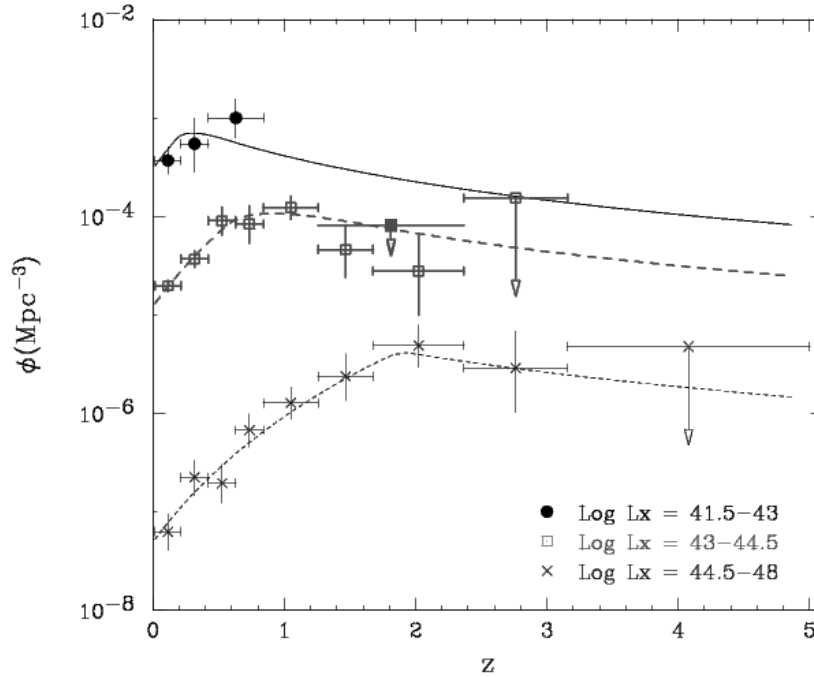


**Fig. 7.** The comoving spatial density of AGN in three X-ray luminosity ranges as a function of redshift, derived using data from several X-ray surveys. From Y. Ueda, M. Akiyama, K. Ohta, et al., 2003, *ApJ*, 598, 886.

Figure 7 shows estimates of the comoving spatial density of AGN in three X-ray luminosity ranges as a function of redshift. These have been constructed utilizing a combination of *Chandra*, *ASCA*, and *HEAO1* surveys at photon energies above 2 keV (with 247 AGN in total). The data are best fit with luminosity-dependent density evolution (LDDE) out to some cutoff redshift ( $z_c$ ), where  $z_c$  increases with luminosity; as a result, the ratio of the peak spatial density to that at the present day is higher for more luminous AGN. At a basic level, LDDE also seems more physically plausible than PLE or PDE; simple PLE models tend to overpredict the number of  $\gtrsim 10^{10} M_\odot$  black holes in the local universe, while simple PDE models tend to overpredict the local space density of quasars.

### 3.3 X-ray Emitting AGN in Luminous Submillimeter Galaxies

The deepest *Chandra* and *XMM-Newton* surveys have finally provided the necessary X-ray sensitivity to complement the most sensitive surveys at submillimeter and infrared wavelengths. One notable instance where obtaining the highest possible X-ray sensitivity has been essential is in studies of the

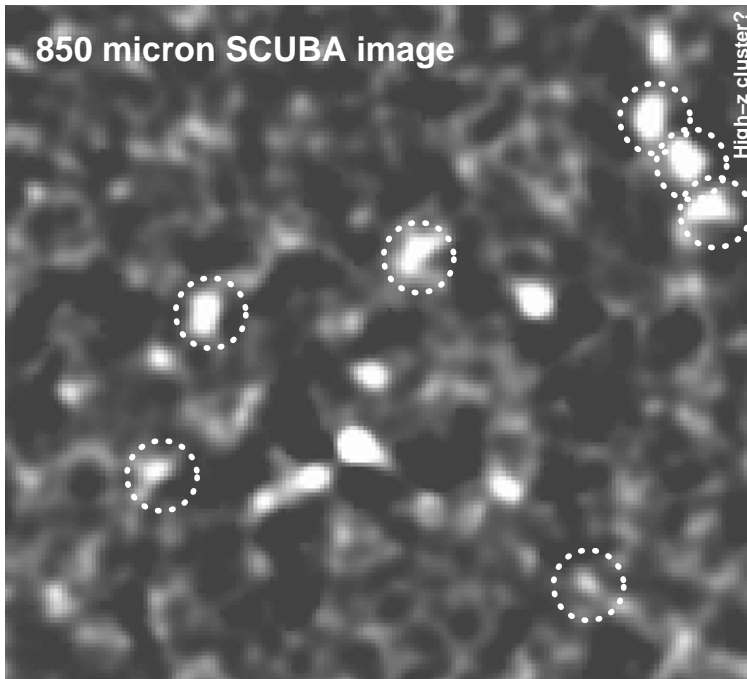


**Fig. 8.** Map at 850  $\mu\text{m}$  of the central region of the CDF-N; the map is  $\approx 6'$  on a side. Sources at 850  $\mu\text{m}$  with X-ray detections are enclosed by dotted circles. The three clustered 850  $\mu\text{m}$ /X-ray sources near the upper-right corner are also coincident with an extended X-ray source, perhaps a high-redshift cluster. Adapted from D.M. Alexander, F.E. Bauer, W.N. Brandt, et al., 2003, *AJ*, 125, 383 and C. Borys, S. Chapman, M. Halpern, et al., 2003, *MNRAS*, 344, 385.

AGN content of distant submillimeter galaxies detected with the SCUBA instrument on the James Clerk Maxwell Telescope. Most of these galaxies are thought to contain intense starbursts with star-formation rates of  $\gtrsim 100 M_{\odot} \text{ yr}^{-1}$ , yet they are not notable in optical galaxy surveys due to dust obscuration of the corresponding starlight. The SCUBA galaxy population is thought to be mostly at  $z \approx 1.5\text{--}3$ , and such galaxies were  $\sim 1000$  times more common at  $z \sim 2$  than in the local universe. The obscured starlight in submillimeter galaxies is re-radiated in the rest-frame infrared (observed-frame submillimeter).

What fraction of submillimeter galaxies contains actively accreting supermassive black holes? Sensitive X-ray studies play an important role in addressing this question, since they allow effective searching for AGN in the majority of submillimeter galaxies that are optically faint (and thus challenging to study in detail with optical spectroscopy). Early comparisons between  $\approx 20\text{--}150$  ks *Chandra* surveys and submillimeter surveys yielded little

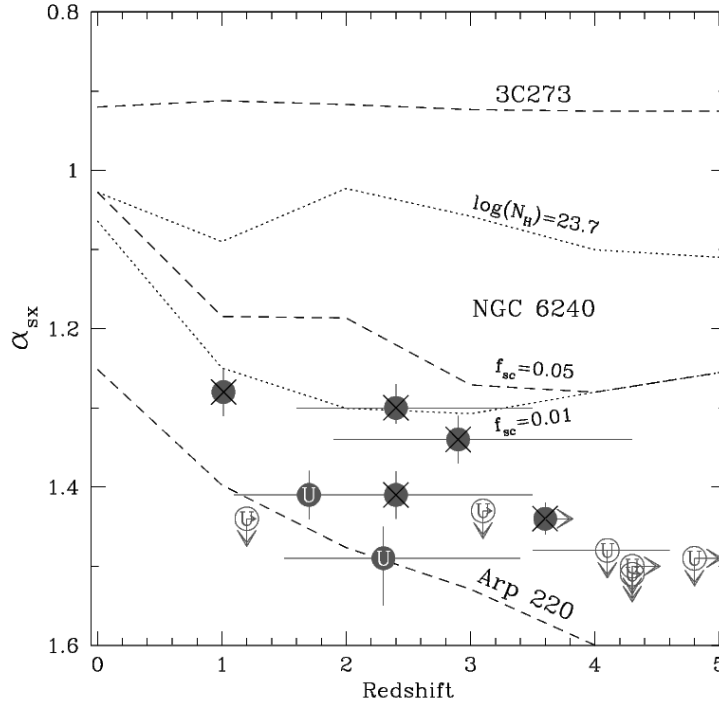


**Fig. 9.** Submillimeter-to-X-ray spectral index ( $\alpha_{\text{sx}}$ ) versus redshift. Submillimeter sources in the central part of the CDF-N with (without) X-ray detections are shown as solid (open) circles. The five circles with overlaid crosses are likely AGN according to their X-ray properties, while those with overlaid “U” are of unknown X-ray type. Dashed curves show  $\alpha_{\text{sx}}$  values for 3C 273, NGC 6240, and Arp 220 adopting their observed amounts of X-ray absorption; alternative dotted curves show an AGN like NGC 6240 but with less internal absorption ( $N_{\text{H}} = 5 \times 10^{23} \text{ cm}^{-2}$ ) and a smaller scattered flux fraction ( $f_{\text{sc}} = 0.01$ ). Adapted from D.M. Alexander, F.E. Bauer, W.N. Brandt, et al., 2003, *AJ*, 125, 383.

( $\lesssim 10\%$ ) source overlap. However, the latest analysis of the 2 Ms CDF-N data reveals that seven of the 13 ( $\approx 54\%$ ) bright submillimeter galaxies (with  $850 \mu\text{m}$  flux densities of  $> 5 \text{ mJy}$ ) in the CDF-N central region mapped with SCUBA have X-ray counterparts (see Figure 8); these counterparts have  $\approx 15\text{--}200$  counts in the full *Chandra* bandpass. Five of the seven X-ray detected submillimeter galaxies likely host obscured AGN based upon their observed X-ray luminosities, X-ray spectral shapes, and X-ray-to-submillimeter flux ratios (see Figure 9). The remaining two have X-ray emission properties consistent with those expected from star formation activity, although it is possible that they host weak AGN as well. If the latter two sources are



indeed powered mainly by star formation, they would be the most X-ray luminous ( $\approx 4 \times 10^{42}$  erg s $^{-1}$ ) starburst galaxies known.

Do the X-ray emitting AGN found in many submillimeter galaxies make a significant contribution to these galaxies' total energy output? Answering this question requires assessment of the amount of X-ray absorption present since, for a given observed X-ray flux, a Compton-thick AGN can be much more luminous than a Compton-thin AGN (see §3.1). Basic X-ray spectral fitting suggests that three of the five submillimeter galaxies hosting AGN in the CDF-N central region have Compton-thin absorption, while only one is likely to have Compton-thick absorption (the final object has poor X-ray spectral constraints). Armed with this knowledge, consideration of the observed X-ray-to-submillimeter flux ratios (see Figure 9) suggests that  $\lesssim 10\%$  of the total energy output from these submillimeter galaxies is ultimately due to an AGN. Star-formation is apparently the dominant power source for the infrared/submillimeter emission, even when an AGN is also present.

The results above are currently being extended, utilizing redshifts from ongoing deep optical spectroscopy. Thus far, these extended results confirm the main conclusions above.

### 3.4 High-Redshift ( $z > 4$ ) AGN Demography and Physics

As is apparent from Figures 5 and 10, deep X-ray surveys can detect  $z > 4$  AGN that are  $\gtrsim 10$ –30 times less luminous than those found in wide-field optical AGN surveys such as the SDSS. At least in the local universe, such moderate-luminosity AGN are much more numerous and thus more representative than the rare, highly luminous quasars. Furthermore, unlike the rest-frame ultraviolet light sampled at  $z > 4$  in ground-based AGN surveys, X-ray surveys suffer from progressively *less* absorption bias as higher redshifts are surveyed. At  $z > 4$ , hard  $\approx 2$ –40 keV rest-frame X-rays are accessed; these can penetrate large column densities up to several  $\times 10^{24}$  cm $^{-2}$ .

Spectroscopic follow-up of moderate-luminosity X-ray detected AGN at  $z > 4$  is challenging, since such objects are expected to have  $z$  magnitudes of 23–26 (provided they have not “dropped out” of the  $z$  bandpass entirely). Nevertheless, significant constraints on the sky density of such objects have been set via large-telescope spectroscopy and Lyman-break selection. In the latter case, objects can be selected that either have appropriate optical/near-infrared colors to be at  $z > 4$  or alternatively have no optical/near-infrared detections. The “bottom line” from these demographic studies in the CDF-N and CDF-S is that there are  $\lesssim 12$  AGN at  $z > 4$  detectable in a 1–2 Ms *Chandra* field, and that only  $\approx 4$  of these have a  $z$  magnitude of  $< 25$  (this limit on the sky density is still  $\sim 260$  times the sky density of  $z > 4$  quasars from the SDSS). These sky-density constraints are sufficient to rule out some pre-*Chandra* predictions by about an order of magnitude, and the combined X-ray and SDSS results indicate that the AGN contribution to reionization at  $z \approx 6$  is small.

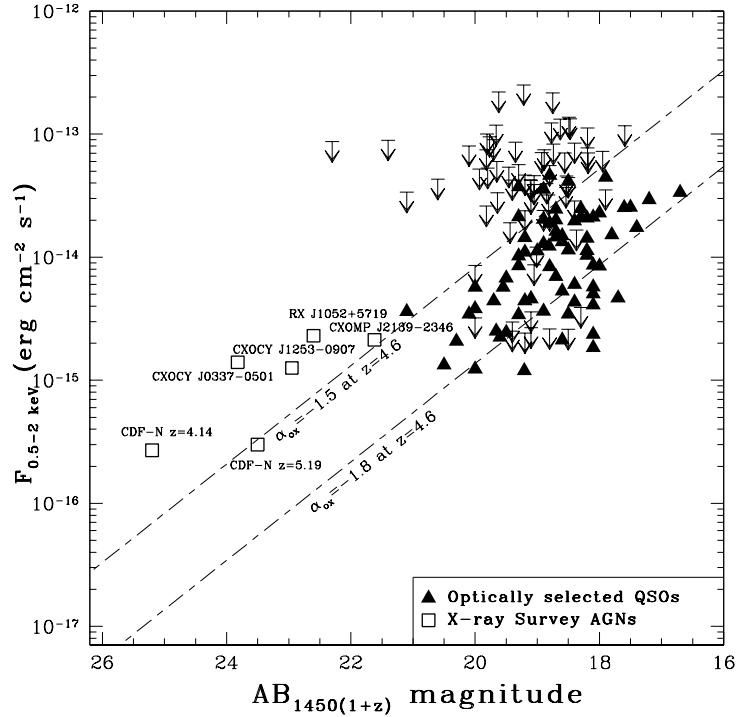


**Fig. 10.** Observed-frame, Galactic absorption-corrected 0.5–2 keV flux versus  $AB_{1450(1+z)}$  magnitude for  $z \geq 4$  AGN found both in optical and X-ray surveys (the X-ray upper limits shown are all for AGN from optical surveys). The slanted, dashed lines show the  $\alpha_{\text{ox}} = -1.5$  and  $\alpha_{\text{ox}} = -1.8$  loci at  $z = 4.6$ . Adapted from C. Vignali, W.N. Brandt, D.P. Schneider, et al., 2003, *AJ*, 125, 2876.

Once high-redshift AGN have been identified, via either X-ray or optical surveys, broad-band spectral energy distribution analyses and X-ray spectral fitting can provide information on their accretion processes and environments. The currently available data, albeit limited, suggest that  $z > 4$  AGN are accreting and growing in roughly the same way as AGN in the local universe; there is no evidence that their inner X-ray emitting regions have been affected by, for example, accretion-disk instabilities or radiation-trapping effects. Figure 10 plots X-ray versus optical flux for  $z > 4$  AGN from both X-ray and optical surveys. The X-ray-to-optical spectral indices,  $\alpha_{\text{ox}}$ , for these objects are consistent with those of AGN in the local universe, once luminosity effects and selection biases are taken into account. These biases and effects likely explain, for example, why the moderate-luminosity, X-ray selected AGN in Figure 10 have notably higher X-ray-to-optical flux ratios than the luminous, optically selected quasars.

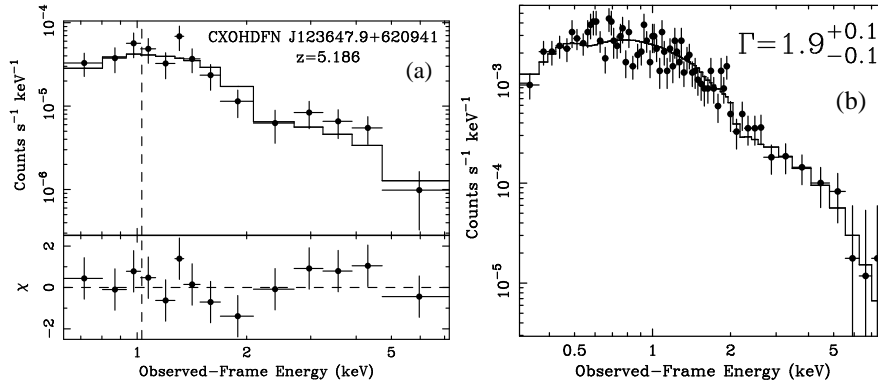


**Fig. 11.** Observed-frame X-ray spectra for (a) the  $z = 5.186$  CDF-N AGN CXOHDFN J123647.9+620941 and (b) 46 radio-quiet quasars at  $z = 4.0-6.3$  that have been stacked together. The best-fitting power-law models with Galactic absorption are also shown; see the text for fitting results. In (a) the lower panel shows the fit residuals in units of sigma, and the vertical dashed line indicates the energy of the (undetected) 6.4 keV iron  $K\alpha$  line. Adapted from C. Vignali, F.E. Bauer, D.M. Alexander, et al., 2002, *ApJ*, 580, L105 and C. Vignali, W.N. Brandt, & D.P. Schneider, 2004, *astro-ph/0310659*.

Two recent X-ray spectral fitting results on  $z > 4$  AGN are shown in Figure 11. Figure 11a shows the X-ray spectrum of the highest redshift AGN discovered thus far in the CDF-N, a low-luminosity quasar at  $z = 5.186$ . It was only possible to obtain a respectable-quality X-ray spectrum for such an object due to the 2 Ms CDF-N exposure. Spectral fitting yields a power-law photon index of  $\Gamma = 1.8 \pm 0.3$ , consistent with observations of similar objects at low redshift, and there is no evidence for intrinsic X-ray absorption. Figure 11b shows a “stacked” spectrum of 46 luminous radio-quiet quasars at  $z = 4.0-6.3$  (their median redshift is  $z = 4.43$ ); this spectrum has 750 counts in total. Joint fitting of the 46 individual spectra, using the Cash statistic, yields a power-law photon index ( $\Gamma = 1.9 \pm 0.1$ ) that is again consistent with observations at low redshift. A fairly tight limit on any intrinsic X-ray absorption of  $N_{\text{H}} \lesssim 9 \times 10^{20} \text{ cm}^{-2}$  is also set. The overall picture emerging, then, is that while the AGN population shows enormous changes in number density over cosmic time, individual AGN X-ray emission regions appear to be remarkably stable entities.

## 4 Some Future Prospects

### 4.1 Future Prospects for Chandra and XMM-Newton

Future prospects for learning more about AGN physics and evolution via X-ray surveys appear wonderful! Follow-up studies for most of the  $\approx 40$  sur-

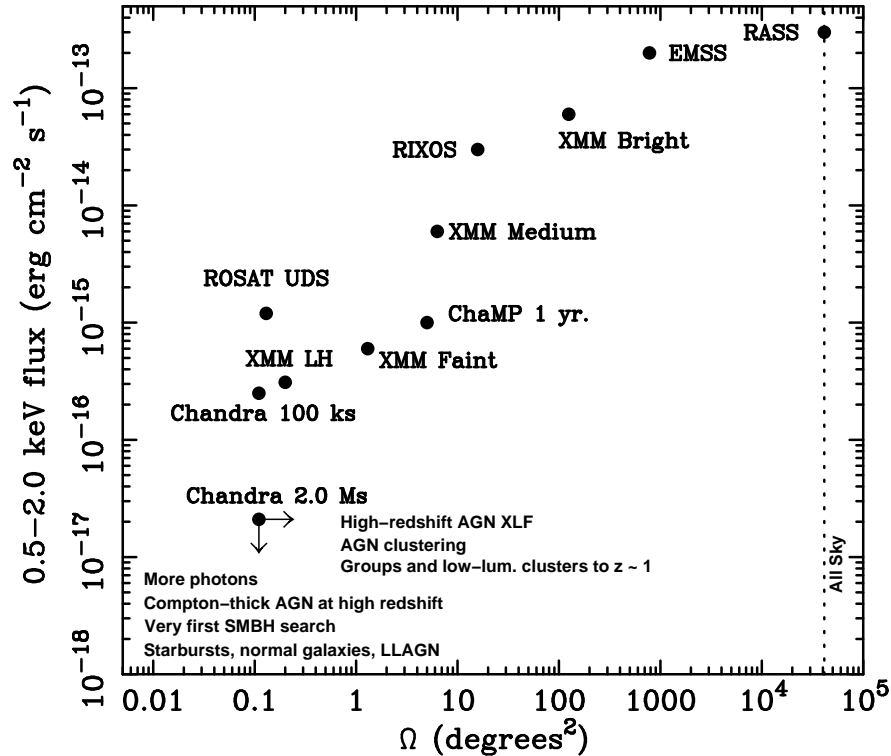


**Fig. 12.** A selection of extragalactic X-ray surveys in the 0.5–2 keV flux limit versus solid angle,  $\Omega$ , plane. Shown are the *ROSAT* All-Sky Survey (RASS), the *Einstein* Extended Medium-Sensitivity Survey (EMSS), the *ROSAT* International X-ray/Optical Survey (RIXOS), the *XMM-Newton* Serendipitous Surveys (*XMM* Bright, *XMM* Medium, *XMM* Faint), the *Chandra* Multiwavelength Project (ChaMP), the *ROSAT* Ultra Deep Survey (*ROSAT* UDS), the  $\approx 100$  ks *XMM-Newton* survey of the Lockman Hole (*XMM* LH), *Chandra* 100 ks surveys, and *Chandra* 2 Ms surveys (i.e., the CDF-N). Although each of the surveys shown clearly has a range of flux limits across its solid angle, we have generally shown the most sensitive flux limit. The vertical dot-dashed line shows the solid angle of the whole sky. Some key science goals achievable by extending deep *Chandra* surveys both wider and deeper are also listed.

veys listed in Table 1 and Table 2 are ongoing, and many exciting results are thus guaranteed even if no more X-ray data are taken. Fortunately, however, both *Chandra* and *XMM-Newton* continue to generate torrents of superb new data that can provide even more impressive advances.

Where can the capabilities of *Chandra* and *XMM-Newton* be best applied in future observations? Figure 12 presents one useful way of thinking about this issue, via a plot of 0.5–2 keV flux limit versus solid angle for selected X-ray surveys. Key parts of this diagram remain to be explored. For

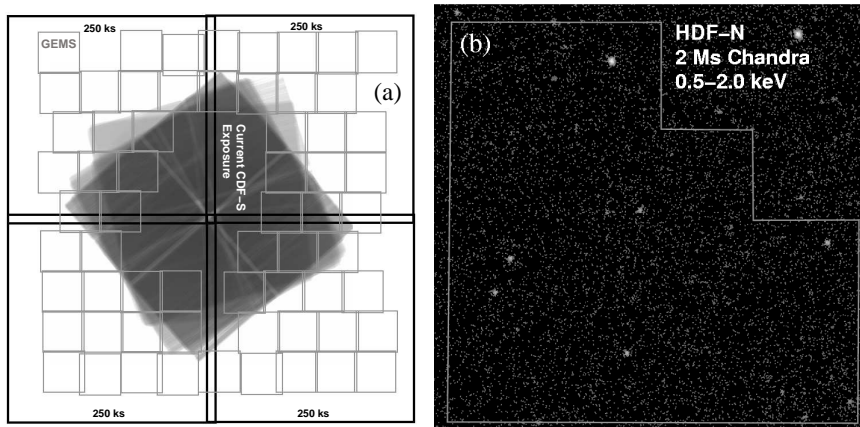


**Fig. 13.** (a) Schematic illustration of the Extended *Chandra* Deep Field-South survey. The underlying grayscale image shows the current CDF-S exposure map. The four large black squares show the coverage of the upcoming four 250 ks *Chandra* observations. The 63 small gray squares show the coverage of *HST* ACS observations made by the GEMS project (the GOODS survey provides *HST* ACS coverage for the central region not covered by GEMS). (b) *Chandra* 0.5–2 keV image of the central part of the 2 Ms CDF-N centered on the HDF-N (shown in outline). Note that most ( $\approx 94\%$ ) pixels are black, indicating no background. *Chandra* is essentially in the photon-limited regime with a 2 Ms exposure, and it can remain in this regime even with an  $\approx 10$  Ms exposure (for 0.5–2 keV sources near the field center).

example, very little solid angle has been surveyed at 0.5–2 keV flux levels of  $(2\text{--}20)\times 10^{-17}$  erg cm $^{-2}$  s $^{-1}$ , and thus our understanding of the X-ray universe at these flux levels suffers from limited source statistics and likely cosmic variance. These flux levels are below the *XMM-Newton* confusion limit, and thus multiple 0.25–2 Ms *Chandra* observations are required. Specific science goals that can be advanced with this approach include (1) pinning down the X-ray luminosity function of moderate-luminosity AGN at  $z \approx 2\text{--}6$ , (2) tracing AGN clustering out to high redshift; this is ideally done with contiguous, deep coverage, and (3) measuring the evolution and properties of groups and low-luminosity clusters out to  $z \approx 1$ . Figure 13a depicts the ongoing Extended *Chandra* Deep Field-South survey, which has been guided by the philosophy above. It will cover a contiguous  $\sim 1/4$  deg $^2$  area at a 0.5–2 keV flux level of  $(1\text{--}2)\times 10^{-16}$  erg cm $^{-2}$  s $^{-1}$ , and it should generate  $\approx 400$  new AGN (in addition to the  $\approx 300$  already known in the CDF-S). Almost all of these will have superb *HST* imaging and multiwavelength coverage.

An equally important guiding philosophy is to observe one field with *Chandra* as sensitively as possible (see Figure 12). Reaching 0.5–2 keV flux levels of  $\approx 5 \times 10^{-18}$  erg cm $^{-2}$  s $^{-1}$  is entirely feasible; *Chandra* could remain nearly photon limited near the field center (see Figure 13b), and source

confusion is unlikely even for source densities exceeding  $100,000 \text{ deg}^{-2}$ . The total required exposure time on a field is  $\approx 10 \text{ Ms}$ . Specific science goals include (1) determining if there is a significant population of Compton-thick AGN at  $z \approx 0.5\text{--}4$  that has been missed to date (see §3.1), (2) tightening constraints on moderate-luminosity AGN at  $z \approx 4\text{--}10$ , (3) detecting hundreds of normal and starburst galaxies out to high redshift (these should outnumber the AGN), and using their X-ray emission as an independent, extinction-free measure of star-formation rate, and (4) obtaining significant numbers of X-ray photons on the faint X-ray source populations currently known, so that X-ray spectral and variability analyses can be applied effectively to determine their nature. Such a sensitive X-ray observation will not be possible again for 10–20 years (see Figure 14)! Performing such an observation now can provide information on the sources that will be the primary targets of future missions such as *XEUS* and *Generation-X*; it will thereby bolster the science cases for these missions and aid their optimal design.

#### 4.2 Upcoming and Planned X-ray Missions

In the future, both large ( $\gtrsim US\$1$  billion, or  $\gtrsim 600$  billion Chilean pesos; see Figure 14) and small-to-medium class ( $\approx US\$120\text{--}180$  million) X-ray missions should substantially advance the AGN X-ray survey work described above. *Constellation-X*, for example, should enable high-quality X-ray spectroscopy for some of the remarkable brighter sources found in X-ray surveys. *XEUS* should be able to generate hundreds of fields that are as sensitive as the deepest *Chandra* surveys, while also providing superior photon statistics to those available presently. Fitting of high-quality *XEUS* spectra should allow direct redshift determination in many cases. Ultimately, *Generation-X* will reach flux limits  $\sim 100$  times better than those of *Chandra* and *XEUS* (see Figure 14). This improved sensitivity should allow detection and study of  $\sim 1000 M_{\odot}$  “proto-quasars” at  $z \approx 10\text{--}15$ , enabling investigation of how the stellar-mass black holes made by the deaths of the first stars grew to make the first AGN.

Future small-to-medium class X-ray missions, at least one to be launched soon, will sensitively survey large areas of sky at high X-ray energies; some will access the poorly explored  $\approx 10\text{--}200 \text{ keV}$  band covering the peak of the XRB. After its 2004–2005 launch, for example, *Swift* will serendipitously conduct the most sensitive  $\approx 10\text{--}150 \text{ keV}$  survey to date with its Burst Alert Telescope. A large fraction of the sky should be covered over the lifetime of *Swift*, and  $\approx 200\text{--}400$  AGN should be detected. In the 2007–2010 timeframe, proposed missions such as the *Dark Universe Observatory (DUO)* and the *Nuclear Spectroscopic Telescope Array (NuSTAR)* will also hopefully conduct sensitive surveys in the  $0.3\text{--}8 \text{ keV}$  and  $6\text{--}80 \text{ keV}$  bands, respectively. *DUO* would detect  $\sim 160,000$  AGN in its surveys of the North Galactic Cap (the SDSS area) and South Galactic Pole, while *NuSTAR* would carry the first highly sensitive, focusing telescope for  $> 10 \text{ keV}$  X-rays. Other planned

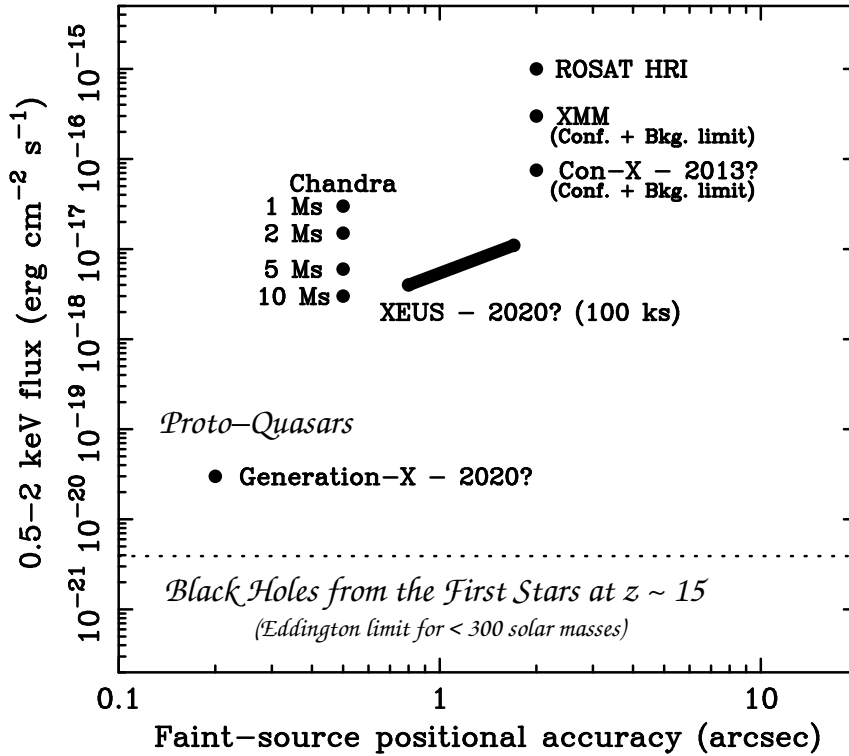


**Fig. 14.** Flux limit from 0.5–2 keV versus faint-source positional accuracy for some past, present, and future X-ray missions (the locations in the diagram and launch dates for future missions are approximate). With a 5–10 Ms exposure, *Chandra* can achieve sensitivities comparable to those discussed for *XEUS*. Furthermore, *Chandra* positions are likely to be the best available for  $\gtrsim 15$  yr. Also shown are the expected X-ray fluxes from (1) the black holes made by the deaths of the first stars at  $z \sim 15$ , and (2) proto-quasars containing black holes of mass  $\sim 10^3$ – $10^4 M_\odot$  at  $z \sim 10$ – $15$ .

small-to-medium class missions include Japan’s *Monitor of All-sky X-ray Image (MAXI)* and *New X-ray Telescope (NeXT)* as well as Europe’s *LOBSTER* and *ROSITA*. The *Black Hole Finder Probe*, defined as part of NASA’s Beyond Einstein program, should ultimately obtain an all-sky census of accreting black holes using a wide-field imaging telescope in the  $\approx 10$ – $600$  keV band.

### Acknowledgments

We gratefully acknowledge support from NSF CAREER award AST-9983783, CXC grant GO2-3187A, the Royal Society (DMA), the PPARC (FEB), and

Italian Space Agency contract ASI/I/R/057/02 (CV). We thank all of our collaborators.

## Some Key Recent References

We have noted the most relevant section above at the end of each reference. Some references are relevant to more than one section; in this case, we have noted the first relevant section. Clearly the relevant literature is extensive, and the reader is urged to consult not only the references below but also the works cited in these references.

- D.M. Alexander, W.N. Brandt, A.E. Hornschemeier, et al., 2001, *AJ*, 122, 2156 (§3.1)
- D.M. Alexander, H. Aussel, F.E. Bauer, et al., 2002, *ApJ*, 568, L85 (§3.1)
- D.M. Alexander, F.E. Bauer, W.N. Brandt, et al., 2003, *AJ*, 125, 383 (§3.3)
- D.M. Alexander, F.E. Bauer, W.N. Brandt, et al., 2003, *AJ*, 126, 539 (§2.1)
- D.M. Alexander, F.E. Bauer, S.C. Chapman, et al., 2004, in *Multiwavelength Mapping of Galaxy Formation and Evolution*, ed. R. Bender, A. Renzini (Springer-Verlag, Berlin), in press (astro-ph/0401129; §3.3)
- O. Almaini, S.E. Scott, J.S. Dunlop, et al., 2003, *MNRAS*, 338, 303 (§3.3)
- A.J. Barger, L.L. Cowie, A.T. Steffen, et al., 2001, *ApJ*, 560, L23 (§3.3)
- A.J. Barger, L.L. Cowie, P. Capak, et al., 2003, *AJ*, 126, 632 (§3.1)
- A.J. Barger, L.L. Cowie, P. Capak, et al., 2003, *ApJ*, 584, L61 (§3.4)
- F.E. Bauer, D.M. Alexander, W.N. Brandt, et al., 2002, *AJ*, 124, 2351 (§3.1)
- A.W. Blain, I. Smail, R.J. Ivison, et al., 2002, *Phys. Rep.*, 369, 111 (§3.3)
- W.N. Brandt, A. Laor, B.J. Wills, 2000, *ApJ*, 528, 637 (§3.1)
- W.N. Brandt, A.E. Hornschemeier, D.M. Alexander, et al., 2001, *AJ*, 122, 1 (§3.1)
- W.N. Brandt, D.M. Alexander, A.E. Hornschemeier, et al., 2001, *AJ*, 122, 2810 (§2.1)
- W.N. Brandt, C. Vignali, D.P. Schneider, et al., 2004, *Adv. Space Res.*, in press (astro-ph/0212082; §3.4)
- S.C. Chapman, A.W. Blain, R.J. Ivison, et al., 2003, *Nature*, 422, 695 (§3.3)
- A. Comastri, M. Mignoli, P. Ciliegi, et al., 2002, *ApJ*, 571, 771 (§3.1)
- L.L. Cowie, A.J. Barger, M.W. Bautz, et al., 2003, *ApJ*, 584, L57 (§3.2)
- S. Cristiani, D.M. Alexander, F.E. Bauer, et al., 2004, *ApJ*, 600, L119 (§3.4)



- S.M. Croom, R.J. Smith, B.J. Boyle, et al., 2004, MNRAS, in press (astro-ph/0403040; §3.2)
- F. Fiore, M. Brusa, F. Cocchia, et al., 2003, A&A, 409, 79 (§3.2)
- P. Gandhi, C.S. Crawford, A.C. Fabian, et al., 2004, MNRAS, 348, 529 (§3.1)
- R. Giacconi, A. Zirm, J.X. Wang, et al., 2002, ApJS, 139, 369 (§2.1)
- M. Giavalisco, H.C. Ferguson, A.M. Koekemoer, et al., 2004, ApJ, 600, L93 (§2.1)
- R. Gilli, 2004, Adv. Space Res., in press (astro-ph/0303115; §3.1)
- P.J. Green, J.D. Silverman, R.A. Cameron, et al., 2004, ApJS, 150, 43 (§2.2)
- G. Hasinger, B. Altieri, M. Arnaud, et al., 2001, A&A, 365, L45 (§2.1)
- A.E. Hornschemeier, W.N. Brandt, G.P. Garmire, et al., 2000, ApJ, 541, 49 (§3.3)
- A.E. Hornschemeier, F.E. Bauer, D.M. Alexander, et al., 2003, AJ, 126, 575 (§3.1)
- A.E. Hornschemeier, D.M. Alexander, F.E. Bauer, et al., 2004, ApJ, 600, L147 (§3.1)
- M.P. Hunt, C.C. Steidel, K.L. Adelberger, et al., 2004, ApJ, in press (astro-ph/0312041; §3.1)
- F. Jansen, D. Lumb, B. Altieri, et al., 2001, A&A, 365, L1 (§1)
- D.W. Kim, R.A. Cameron, J.J. Drake, et al., 2004, ApJS, 150, 19 (§2.2)
- A.M. Koekemoer, D.M. Alexander, F.E. Bauer, et al., 2004, ApJ, 600, L123 (§3.4)
- A. Marconi, G. Risaliti, R. Gilli, et al., 2004, MNRAS, in press (astro-ph/0311619; §3.1)
- G. Matt, 2002, Phil. Trans. R. Soc. Lond. A, 360, 2045 (§3.1)
- G. Matt, A.C. Fabian, M. Guainazzi, et al., 2000, MNRAS, 318, 173 (§3.1)
- E.C. Moran, A.V. Filippenko, R. Chornock, 2002, ApJ, 579, L71 (§3.1)
- R.F. Mushotzky, L.L. Cowie, A.J. Barger, et al., 2000, Nature, 404, 459 (§2.1)
- B.M. Peterson, 1997, An Introduction to Active Galactic Nuclei (Cambridge University Press, Cambridge), pp. 183–193 (§3.2)
- G. Risaliti, R. Maiolino, M. Salvati, 1999, ApJ, 522, 157 (§3.1)
- H.-W., Rix, M. Barden, S.V.W. Beckwith, et al., 2004, ApJ, in press (astro-ph/0401427; §4.1)
- M. Schmidt, 1968, ApJ, 151, 393 (§3.2)
- D.P. Schneider, X. Fan, P.B. Hall, et al., 2003, AJ, 126, 2579 (§3.4)
- P. Severgnini, A. Caccianiga, V. Braitto, et al., 2003, A&A, 406, 483 (§3.1)
- I.A.G. Snellen, P.N. Best, 2001, MNRAS, 328, 897 (§3.1)
- A.T. Steffen, A.J. Barger, L.L. Cowie, et al., 2003, ApJ, 596, L23 (§3.2)
- G.P. Szokoly, J. Bergeron, G. Hasinger, et al., 2004, ApJS, submitted (astro-ph/0312324; §3.1)

- Y. Ueda, M. Akiyama, K. Ohta, et al., 2003, *ApJ*, 598, 886 (§3.1)
- C. Vignali, F.E. Bauer, D.M. Alexander, et al., 2002, *ApJ*, 580, L105 (§3.4)
- C. Vignali, W.N. Brandt, D.P. Schneider, 2003, *AJ*, 125, 433 (§3.4)
- C. Vignali, W.N. Brandt, D.P. Schneider, et al., 2003, *AJ*, 125, 2876 (§3.4)
- M.C. Weiskopf, H.D. Tananbaum, L.P. Van Speybroeck, et al., 2000, *Proc. SPIE*, 4012, 2 (§1)
- R.E. Williams, B. Blacker, M. Dickinson, et al., 1996, *AJ*, 112, 1335 (§2.1)
- C. Wolf, L. Wisotzki, A. Borch, et al., 2003, *A&A*, 408, 499 (§3.2)
- D.G. York, J. Adelman, J.E. Anderson, et al., 2000, *AJ*, 120, 1579 (§3.4)
- F. Yuan & R. Narayan, 2004, *ApJ*, in press (astro-ph/0401117; §3.1)